The Structure of Alkali Tellurite Glasses

J. C. McLaughlin,* S. L. Tagg,† and J. W. Zwanziger‡

Department of Chemistry, Indiana University, Bloomington, Indiana 47405

Received: July 19, 2000; In Final Form: October 11, 2000

Structural models of alkali tellurite glasses, $(M_2O)_x(TeO_2)_{1-x}$ with M = Li, Na, K are presented. The glass structure was studied with neutron and X-ray diffraction, and, in the case of sodium, NMR. Real-space models of the glass structure were built using the reverse Monte Carlo algorithm. The distribution of polyhedral types as a function of alkaline ion type and composition is derived. It is concluded that the broad distribution of polyhedral species, as compared to that found in crystalline tellurites of similar composition, is responsible for the marked resistance to devitrification shown by these glasses.

1. Introduction

Glass-forming oxides typically include a network former, such as silica, and a modifier, such as sodium oxide. The distinction between these species may be understood, at least at an empirical level, as arising from their relative field strengths.[1] Network formers, viewed as ions in an oxide solid, exhibit quite high field strengths, whereas modifier field strengths are low. The network formers thus dominate the structure, giving rise to the well-defined polyhedra observed in the classical glasses, such as $SiO_{4/2}$ in SiO_2 and $BO_{3/2}$ in B_2O_3. These compounds thus yield stable disordered solids, which presumably are stable against devitrification because the energetics are dominated to a great extent by short-range interactions, so that devitrification would require significant breaking and re-forming of network connections. In contrast, the modifiers weaken the structure by replacing strongly coordinating network formers with weakly interacting modifiers. Additionally, modifiers are always introduced in conjunction with oxide, so that as the network formers maintain their local polyhedral environments, nonbridging oxygens are necessarily introduced. This addition leads to lower network connectivity and typically reduced glass transition temperatures. Modifiers on their own do not form glasses, again presumably because the solids easily devitrify by rearrangement to crystalline forms.

It is of fundamental importance in glass science to understand the structural forms that arise in glasses composed of network formers of intermediate strength. Furthermore, because the chemistry of intermediate cases is comparatively rich, a wider variety of tunable properties may be found in glasses of this type. In this contribution we focus on simple tellurite glasses.

Because of its large ionic radius, the field strength of Te^{IV} is intermediate between the good glass formers and the modifiers. Indeed, telluria (TeO_2) is only a conditional glass former and requires fast-quenching techniques to form a glass. The resulting amorphous material is not stable with respect to devitrification, in marked contrast to other typical network glass formers such as SiO_2, P_20_5, and B_2O_3.[1] Surprisingly, therefore, addition of alkali oxides to TeO_2 results in glasses that require only modest cooling rates for preparation. These glasses can be prepared across relatively large compositional ranges of added modifier (Table 1) and are quite resistant to devitrification.[2] This resistance peaks at about 20 mol-% modifier. Additionally, alkali tellurite glasses have strikingly high nonlinear optical susceptibility,[3] excellent chemical durability,[1] and are the basis for a potentially important family of optically active, transparent glass ceramics.[4]

TABLE 1: Glass Forming Region and Crystal Compositions in Terms of Mole Fraction M_2O for Alkali Tellurite Glasses $(M_2O)_x(TeO_2)_{1-x}$

modifier	glass-forming region		crystalline compositions	
M_2O	Mochida[35]	Vogel[36]	M_2O fraction	ref
Li_2O	0.10−0.25	0.12−0.35	0.33 (α,β), 0.50	37, 38, 39
Na_2O	0.05−0.30	0.055−0.38	0.20, 0.33, 0.50	37, 38, 39
K_2O	0.025−0.25	0.065−0.195	0.20, 0.33, 0.50	22, 42
Rb_2O	0.03−0.25	0.056−0.21	no data	
Cs_2O	no data	no data	0.20, 0.33, 0.50	43

In other glass-forming systems, anomalous behavior in bulk properties as a function of composition can usually be explained on the basis of the glass structure. For example, the initial increase in glass transition temperature with added modifier in borates is due to the formation of BO_4 units, which add strength to the network despite the modifier addition. Similarly, modification of GeO_2 glass proceeds initially by formation of GeO_6 octahedra. The glass transition temperature and molar volume in tellurites do not show similar anomalies, but the resistance to devitrification does, as noted above.[2] This observation suggests that the network is cleaved by the addition of modifier in the conventional way, but that some other structural features add resistance to devitrification. We hypothesized that the wide variety of tellurite polyhedra, observed in crystal structures of alkali tellurites, plays a role in stabilizing the glasses. This paper reports the results of testing this hypothesis. The physical properties and structural changes in alkali tellurite glasses as a function of modifier identity and content have been studied by a variety of experimental techniques including IR,[5] neutron diffraction,[6−9] X-ray diffraction,[10] Mössbauer spectroscopy,[11] Raman scattering,[12−14] and NMR.[15−18] Structural units within tellurite glasses have also been modeled quantum mechanically.[19−21] To provide a unified overview of this body of work, as well as to provide a succinct presentation of our own results, we will denote the tellurite polyhedra by Q^n_m, where the

* Present address: NIST Center for Neutron Research, National Institute of Standards and Technology, Gaithersburg, MD 20899-8562

† Present address: Micron Technology, Inc., Boise ID 83707-0006.

‡ Corresponding Author. Tel: (812) 855-3994; Fax: (812) 855-8300; E-mail: jzwanzig@indiana.edu.

10.1021/jp0025779 CCC: $20.00
Published on Web 12/15/2000

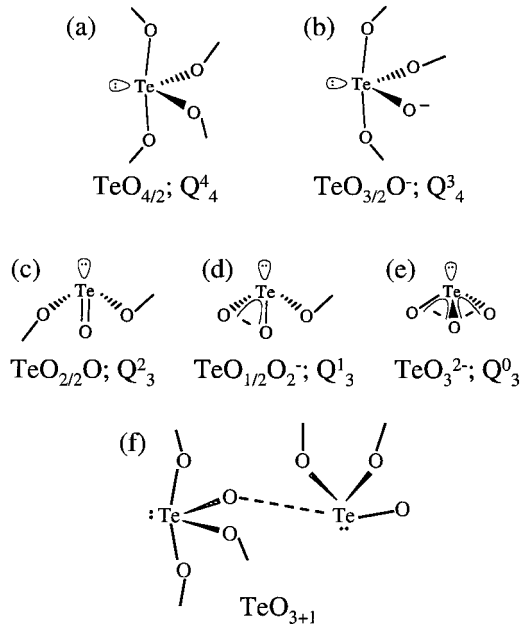

Figure 1. (a−e) Five basic tellurite units found in alkali tellurite crystals.[22] They are labeled according to both the conventional nomenclature and the Q^n_m nomenclature discussed in the main text. (f) TeO_{3+1} distorted tbp where one Te−O bond is significantly longer then the other three bonds. The Te_{3+1} unit is often used as an intermediate between TeO_4 tbp and TeO_3 tp when describing tellurite glass structure.

superscript n gives the number of bridging oxygen, and the subscript m is the coordination number. Examples are shown in Figure 1.

The first neutron diffraction experiment on alkali tellurite glasses, by Neov et al.[6] on a lithium tellurite glass, $(Li_2O)_{0.2}$-$(TeO_2)_{0.8}$, collected data only out to $Q = 10$ Å^{-1}, and only one peak was observed between 1.9 and 2.0 Å in the pair distribution function (PDF). This peak was assigned to Te−O. The calculated Te−O coordination number was ≈4, leading Neov et al. to suggest that the Te−O network underwent a rearrangement rather than cleavage into TeO_3 trigonal pyramids (tp). Later studies by Suzuki et al.[7,8] on $(BaO)_x(TeO_2)_{1-x}$ glasses collected data to $Q = 30$ Å^{-1} and succeeded in resolving two peaks in the PDF, at 1.9 and 2.2 Å. From the peak intensities, the $TeO_{4/2}$ units were described as distorted trigonal bipyramids (tbp) with three short Te−O bonds and one long Te−O bond, which is written as TeO_{3+1}. As the mole fraction of BaO increased, the intensity of the second peak decreased, leading Suzuki et al. to conclude that the glass is gradually broken up from distorted TeO_{3+1} units to TeO_3 trigonal pyramids.

By comparing the Raman scattering in alkali tellurite crystals, TeO_2 glass, and alkali tellurite glasses, Sekiya et al.[12] assigned the Raman modes to specific structural units and proposed a scheme for the conversion of the TeO_4 tbp's to TeO_{3+1} and finally to TeO_3 tp's. Tatsumisago et al.[13] studied $(Li_2O)_x(TeO_2)_{1-x}$ as a function of modifier and temperature and interpreted the results in terms of the breakup of the tellurite network from TeO_4 tbp to TeO_3 tp. A third Raman study by Himei et al.[14] proposed a model based on two equilibria:

$$TeO_{4/2}\ (Q^4_4) \rightleftharpoons O_{2/2}TeO\ (Q^2_3)$$

$$O_{3/2}TeO^-\ (Q^3_4) \rightleftharpoons O_{1/2}TeO_2^-\ (Q^1_3)$$

Unfortunately the Raman data do not provide enough information to calculate the composition of the glass in terms of the four species identified.

In a recent series of NMR experiments, Sakida et al. used ^{125}Te NMR to investigate tellurite crystals[17] and glasses.[18] On the basis of studies of a variety of tellurite crystals (but none of composition overlapping the glasses studied), they correlated the NMR line shapes with coordination number. The data are used in conjunction with the model developed by Himei et al. but with one major difference: the Q^2_3 unit is explicitly excluded. Their justification is based on an ab initio cluster model calculation done by Uchino et al.[19] which predicts Raman modes for Q^2_3 at 775 and 870 cm-l; these bands are not observed in TeO_2 glasses measured by Tatsumisago et al.[13] By eliminating Q^2_3 as a variable, the model allows the calculation of the distribution of species from the Te−O coordination number and a charge balance constraint. Our results will show that excluding the Q^2_3 unit is an oversimplification of the alkali tellurite glass structure, details of which are saved for the discussion section.

We have taken an approach to determining the structure of tellurite glasses that relies heavily on knowledge of structures found in crystalline tellurites. While glasses lack the long-range order characteristic of crystals, the chemical forces controlling the short-range order are similar. Therefore, insight into glass structure is gained by examining the crystal phases of similar composition. The relevant crystal structures in the alkali tellurite system are listed in Table 1, and a discussion of the crystal chemistry can be found in ref 22. Five basic tellurite units (Figure 1 a−e) were identified in the crystal structures.

Concurrent with the work on the crystal structures, we probed the alkali atom environments in sodium tellurite glasses with two NMR experiments. A dynamic angle spinning (DAS) NMR experiment[15] provided information about the chemical shift of the sodium. The chemical shift can be related empirically to the number of near-neighbor oxygen atoms atoms surrounding each sodium atom,[15,23] resulting in a measurement of the Na−O average coordination number. The second NMR experiment[16] measured the second moment (M_2) of the distribution of sodium−sodium dipolar couplings. The second moment is related to the distance between sodium nuclei and the orientation of the internuclear vector relative to the applied magnetic field. Previously we have related the second moment to the sodium−sodium pair-correlation function,[16] allowing M_2 to be used as a constraint in the reverse Monte Carlo (RMC) algorithm.[24]

In the following, we will describe the diffraction experiments that were performed to study the glass structure and the models that were constructed to account for the diffraction data (and, where available, the NMR data). The resulting models are then analyzed to give the distribution of polyhedral types present in the glasses. The dependence on modifier size is demonstrated, and finally conclusions are drawn concerning the relation of the glass stability to its structure.

2. Methods

2.1. Sample Preparation. Samples of alkali tellurite glasses were prepared by melting alkali carbonate and tellurite together at 800 °C for 15 min (by which time CO_2 evolution had ceased). The liquids were quenched between steel or brass plates. Sample composition was determined by weight-loss measurements and in some cases by electron microprobe analysis. The final compositions are precise to within ±1%. The glass transition temperatures were found by differential scanning calorimetry and agreed within experimental error with previously published data.

2.2. Data Acquisition. Neutron diffraction was measured on the glass, liquid, and amorphous diffractometer (GLAD) at the

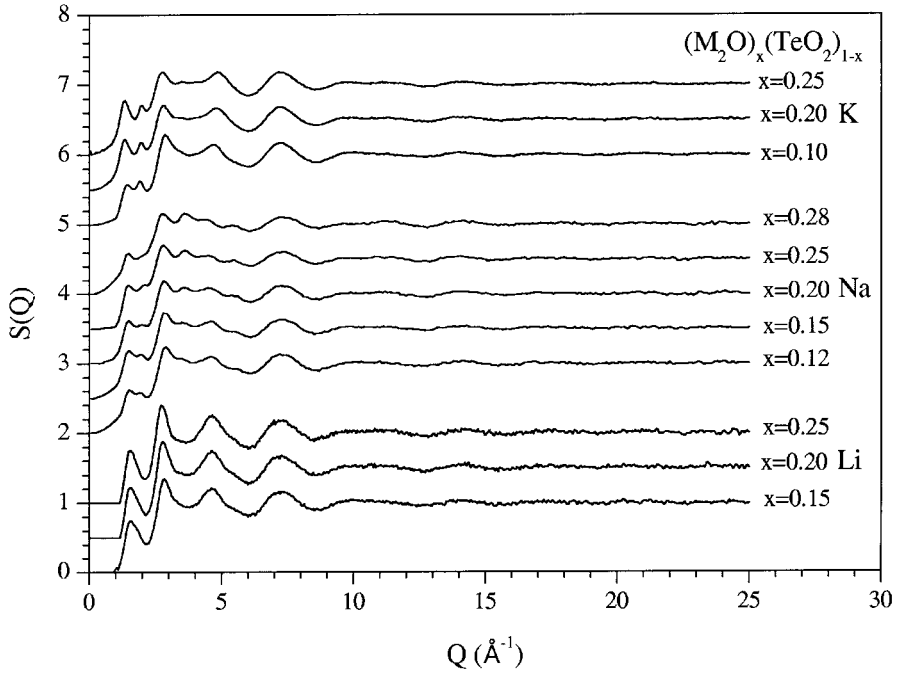

Figure 2. Total static structure factor $S(Q)$ from neutron diffraction measurements for alkali tellurite glasses, $(M_2O)_x(TeO_2)_{1-x}$, M = Li, Na, or K. Each $S(Q)$ is shifted upward by 0.5 units between each composition and by 1 unit between different cations.

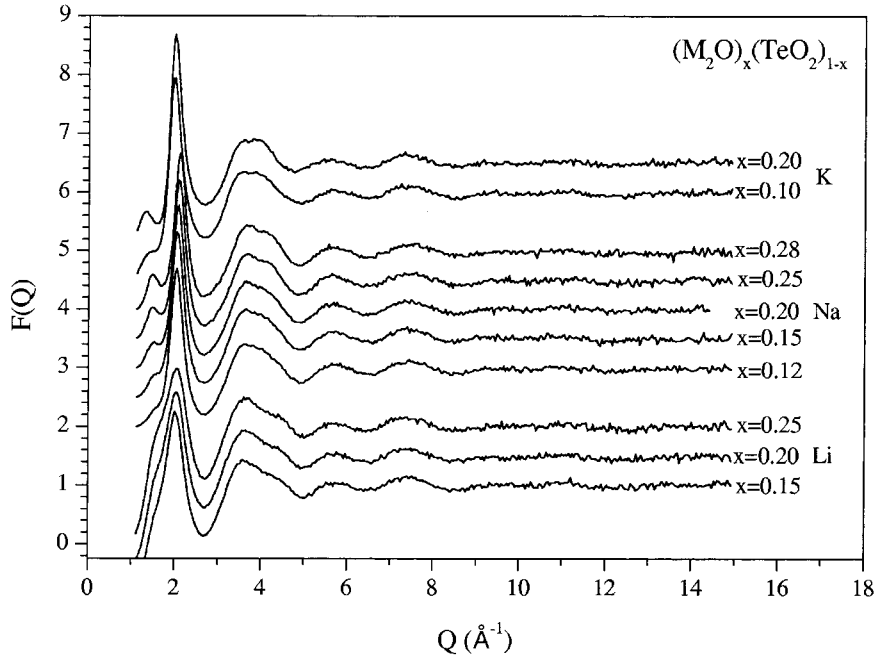

Figure 3. $F(Q)$ from X-ray diffraction measurements for alkali tellurite glasses, $(M_2O)_x(TeO_2)_{1-x}$, M = Li, Na, or K. Each $F(Q)$ is shifted upward by 0.5 units between each composition and by 1.0 units between different cations.

Intense Pulsed Neutron Source, Argonne National Laboratory (Figure 4). This time-of-flight instrument has been described previously.[25] For each sample, the total static structure factor was extracted from the data using standard codes optimized for the GLAD instrument. The only nonstandard feature used was a 0.286 Å cutoff of the neutron energy to remove the tellurium neutron absorption resonance at 1.0 eV. For each sample the total structure factor, $S(Q)$, was extracted after correcting the raw data for background artifacts, inelastic scattering, and multiple scattering, using the suite of programs designed for the GLAD instrument.[25]

X-ray diffraction was performed on the Sector 1 bend-magnet beam line (1-BM), operated by the Synchrotron Research and Instrumentation Collaborative Access Team (SRI−CAT) at the Advanced Photon Source, Argonne National Laboratory (Figure 6). In order to be well above all absorption resonances, achieve wide Q-space coverage, and yield predominantly interior rather than surface diffraction, 61.332 keV photons were used. The photons were selected with a single Si(111) crystal with a 1.6° miscut. The crystal was bent (meridionally) to a monochromatic focus at the detector position. The monochromator crystal deflection was horizontal, while the scattering plane for the sample/detector was vertical in order to preserve acceptable angular resolution. A Ge solid-state detector was used. The structure factor, $F(Q)$, was extracted from the data, by correcting for Compton scattering, absorption, polarization, and background

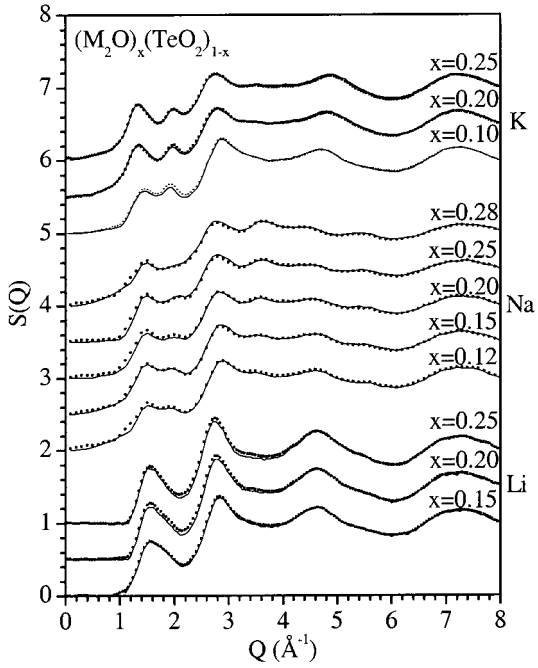

Figure 4. Model fit (dotted line) to the total static structure factor $S(Q)$ (solid line) from neutron diffraction for the different compositions $(M_2O)_x(TeO_2)_{1-x}$, M = Li, Na, or K. Each $S(Q)$ is shifted upward by 0.5 units between each composition and by 1 unit between different cations.

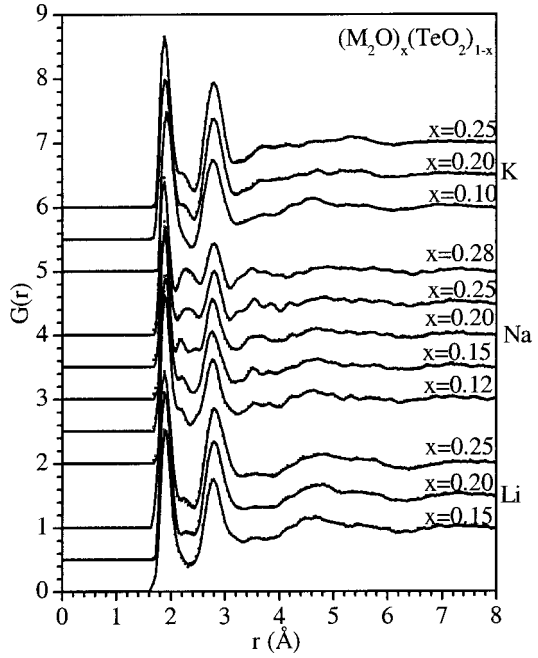

Figure 5. Model fit (dotted line) to the total pair-correlation function $G(r)$ (solid line) from neutron diffraction for the different compositions $(M_2O)_x(TeO_2)_{1-x}$, M = Li, Na, or K. Each $G(r)$ is shifted upward by 0.5 units between each composition and by 1 unit between different cations.

diffraction, following the procedure outlined by Williams.[26] The instrument dead-time was also measured and compensated for in the data analysis.

2.3. Model Construction. The RMC simulations were performed using a modified version[24] of the original RMC code.[27−29] The RMC models were built using 3750 atoms in a cubic box. A minimum approach distance R_{ij}^{min} between atoms was applied using the values shown in Table 2. General

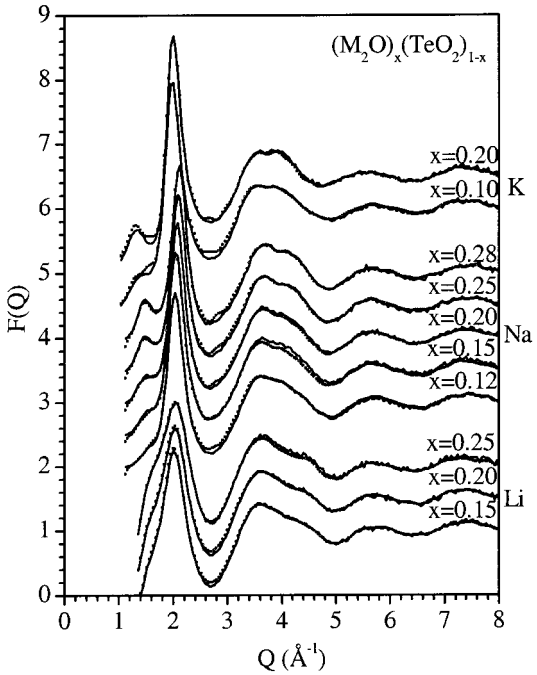

Figure 6. Model fit (dotted line) to the total static structure factor $F(Q)$ (solid line) from X-ray diffraction for the different compositions $(M_2O)_x(TeO_2)_{1-x}$, M = Li, Na, or K. Each $F(Q)$ is shifted upward by 0.5 units between each composition and by 1 unit between different cations.

TABLE 2: Coordination Numbers Calculated between R_{ij}^{min} and R_{ij}^{max}, Which Were Determined from the Crystal Structures

modifier		Te−Te	Te−M	Te−O	M−M	M−O	O−O
M = Li	R_{ij}^{min}	3.08	3.0	1.68	2.52	1.8	2.48
	R_{ij}^{max}	4.72	4.0	2.36	3.5	2.2	3.6
M = Na	R_{ij}^{min}	3.08	3.16	1.68	3.08	2.16	2.48
	R_{ij}^{max}	4.72	4.0	2.36	4.0	3.20	3.6
M = K	R_{ij}^{min}	3.08	3.24	1.68	3.36	2.48	2.48
	R_{ij}^{max}	4.72	4.5	2.36	4.5	3.12	3.6

coordination constraints were applied to generate the correct chemistry for tellurium (3 or 4 coordinate), oxygen (1 or 2 coordinate), and M−O (variable coordination for sodium, based on NMR data,[15] and 3.5 coordinate for lithium and 6.5 coordinate potassium, based on the crystal structures[22]). The models were then fit to the diffraction data in the order *G(r)*, *S(Q)*, and *F(Q)*. Finally, a constraint was added to limit the tellurite units (Q_3^2) to those found in the crystal structures[22] (Figure 1). For the sodium tellurite glasses only, an additional constraint on the Na−Na *G(r)* based on *M2* NMR measurements16 was added. Details about the modified code for the Q_3^2 constraint and the M_2 constraint have been published elsewhere.[24]

3. Results

The total structure factors, $S(Q)$, for the neutron diffraction experiments are shown in Figure 2, and the total structure factors, *F(Q)*, from X-ray experiments are shown in Figure 3. The fits from the RMC models to the experimental data for $S(Q)$, *F(Q)*, and *G(R)*, the transform of *S(Q)*, are shown in Figures 4−6, respectively. In all cases the RMC models provide excellent fits, indicating that the assumptions in the models are consistent with the experimental data.

TABLE 3: Faber−Ziman Weighting Coefficients W_{ij} of Each Atom Pair in the Total Neutron Structure Factor $S(Q)$ and the Comparable Weights at $Q = 0$ for the Total X-ray Diffraction Structure Factor $F(Q)$[a]

atom pair	W_{ij} (neutrons)	W_{ij} (X-rays)
Te−Te	0.079	0.481
Te−Na	0.049	0.098
Te−O	0.355	0.327
Na−Na	0.007	0.005
Na−O	0.110	0.033
O−O	0.400	0.056

[a] Values are for the $x = 0.20$ sodium tellurite glass.

TABLE 4: Q-Space and Real-Space Positions for the Peaks in $S(Q)$ and $F(Q)$ for the $x = 0.20$ Alkali Tellurite Glasses Taken from Figure 7

glass	feature in $S(Q)$	Q(A-1)	r(A)
$(Li_2O)_{0.2}(TeO_2)_{0.8}$	peak 1	1.55	4.05
	peak 2		
	peak 3	2.8	2.25
$(Na_2O)_{0.2}(TeO_2)_{0.8}$	peak 1	1.5	4.2
	peak 2	2.0	3.15
	peak 3	2.8	2.25
$(K_2O)_{0.2}(TeO_2)_{0.8}$	peak 1	1.35	4.6
	peak 2	2.0	3.15
	peak 3	2.8	2.25

4. Discussion

Diffraction studies of glasses are complicated due to the overlapping contributions of the pair correlation functions. For the three component systems considered here, full resolution would require six pair-correlation functions, which could be obtained only from six different diffraction experiments. These could be acquired in principle by isotope substitution measurements. However, while isotopes are abundant for Li, they are available but expensive for K, O, and Te, and no stable isotopes exist for Na. We chose instead to use a combination of neutron scattering and X-ray scattering, along with RMC modeling, which allows us to include information from the crystal structures and NMR experiments. The combination of neutron and X-ray scattering is complementary for alkali tellurite glasses since each technique emphasizes different pair-correlation functions, as shown in Table 3 for the $x = 0.20$ sodium tellurite glass. The relative scattering contributions for lithium and potassium tellurite glasses is similar. Table 3 shows that neutron scattering emphasizes the O−O, Te−O, and M−O pair-correlation functions and X-ray scattering emphasizes the Te−Te, Te−O, and Te−M pair-correlation functions.

4.1. First Sharp Diffraction Peak. Examination of *S(Q)* and *F(Q)* (Figure 4 and Figure 6) reveals several trends as a function of both modifier and composition. In many glass systems, neutron and X-ray diffraction data show a feature at low Q values, often referred to as the "first sharp diffraction peak" (FSDP). The FSDP is often considered a manifestation of medium-range order (ordering beyond the first coordination sphere) in covalent glasses, because a peak in $S(Q)$ or *F(Q)* at Q_{FSDP} corresponds to a correlation in real space with a length scale $2\pi/Q_{FSDP}$. In other words, for real space correlations between 4 and 10 Å (typical of intermediate-range order), one expects Q_{FSDP} values between 0.63 and 1.57 $Å^{-1}$. Table 4 gives the position in both Q space and real space for the first three peaks in $S(Q)$ and *F(Q)* for the $x = 0.20$ glasses.

The first peak appears as a small shoulder in the *F(Q)* data and as the first of a pair of small peaks in the $S(Q)$ data. From Figure 7 we see that the Te−O and O−O interactions are primarily responsible for this feature. The feature increases in intensity as a function of added modifier, indicating that the modifier is significant in inducing the structural feature represented by this peak. The peak shifts to lower Q values (larger r values) as the modifier changes from Li to K, suggesting that the Te−O and O−O distances responsible for it increase with increasing cation size. Because the distance in real space is significantly larger than the Te−O bond distance, this shift must be due to a general increase in the second neighbor distances. We interpret the increase as being due to network expansion to accommodate the cation (in agreement with the increase in molar volume with cation size observed in tellurites[3]).

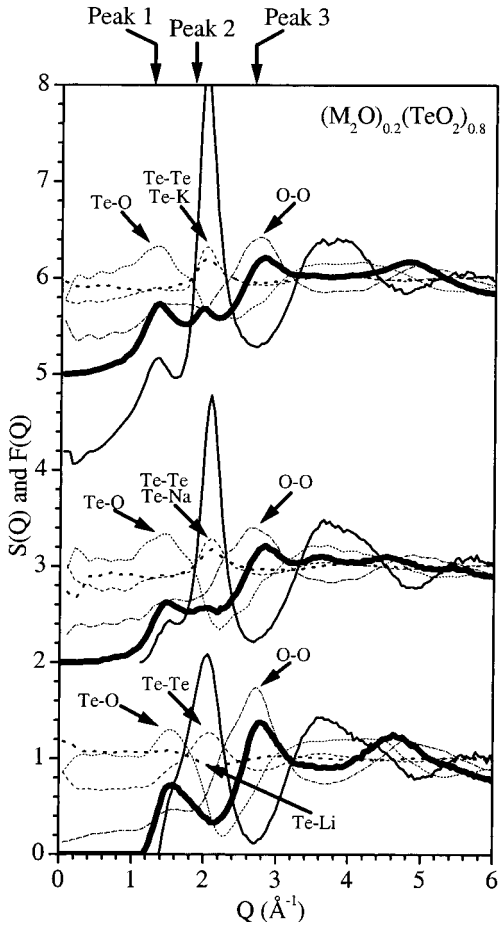

Figure 7. Experimental $S(Q)$ (bold line), $F(Q)$ (solid line), and the partial $S(Q)_{ij}$ from the RMC models for the $x = 0.20$ alkali tellurite glasses. The partials shown are Te−Te (long dash); Te−O (dotted); Te−M (short bold dash); and O−O (dash−dot).

The second peak is the most intense peak in the *F(Q)* data, while appearing only as a small peak in the *S(Q)* data for the Na and K glasses and is mostly absent in the Li glasses. Its prominence in *F(Q)* leads us to identify this feature as due to Te−Te correlations. The feature corresponds to a distance $r =$ 3.2 Å, which is a typical Te−Te distance for corner-sharing units, and is observed in all of the tellurite crystals studied. The peak is very intense in the X-ray data because Te−Te correlations account for ~50% of the intensity, whereas in the neutron data they account for <10%. The feature shows a small dependence on the amount of added modifier (most notable in the sodium tellurite glasses), shifting to slightly higher Q as the fraction of modifier increases. This shift would indicate a small decrease in the average Te−Te distance as the modifier content increases. As a function of modifier identity the feature is unchanged between Li and Na glasses but shifts noticeably to lower Q for the K glasses, indicating that the Te−Te distance

TABLE 5: Coordination Numbers from the RMC Models for Alkali Tellurite Glasses Where M =Li, Na, or K

composition	Te−Te	Te−O	O−Te	O−O
$(Li_2O)_{0.15}(TeO_2)_{0.85}$	8.35	3.53	1.62	7.76
$(Li_2O)_{0.20}(TeO_2)_{0.80}$	7.90	3.44	1.53	7.46
$(Li_2O)_{0.25}(TeO_2)_{0.85}$	7.39	3.49	1.50	7.62
$(Na_2O)_{0.12}(TeO_2)_{0.88}$	7.89	3.64	1.70	7.23
$(Na_2O)_{0.15}(TeO_2)_{0.85}$	7.47	3.57	1.64	6.70
$(Na_2O)_{0.20}(TeO_2)_{0.80}$	7.11	3.57	1.59	6.79
$(Na_2O)_{0.25}(TeO_2)_{0.75}$	6.51	3.57	1.54	6.52
$(Na_2O)_{0.28}(TeO_2)_{0.72}$	6.37	3.64	1.53	6.75
$(K_2O)_{0.10}(TeO_2)_{0.90}$	8.03	3.46	1.64	6.47
$(K_2O)_{0.20}(TeO_2)_{0.80}$	6.31	3.29	1.46	5.44
$(K_2O)_{0.25}(TeO_2)_{0.85}$	5.16	3.17	1.36	4.53

increases. We attribute this change to a slight expansion of the network to accommodate the larger potassium cation.

The third feature is almost entirely absent in the *F(Q)* data, while being the most intense feature in the *S(Q)* data. From the RMC models we see that this feature is mainly due to O−O correlations. The peak is prominent in the *S*(*Q*) data because O−O distances account for ∼40% of the intensity and is absent from the *F(Q)* data because O−O distances only account for ∼6% of the intensity. The corresponding distance in real space is $r = 2.25$ Å, which corresponds well to typical O−O distances seen in alkali tellurite crystals for oxygen bonded to the same tellurium atom. The intensity of the peak decreases slightly and shifts to lower *Q* values as modifier is added, though the identity of the modifier does not appear to be important. This shift could indicate a slight increase in the O−O distance as modifier is added.

4.2. Coordination Numbers. Because of the overlapping bond length ranges in these glasses, we extracted coordination numbers from the RMC models rather than directly from the neutron and X-ray diffraction data. In simpler systems, Gaussians can be fit to peaks in the total correlation functions which have been assigned to particular bonding pairs. Then, from the peak areas, the composition and scattering properties, coordination numbers can be obtained. Here we focused directly on the real space models to obtain this information, because of the peak overlap in the diffraction data.

The coordination numbers are listed in Table 5. The coordination numbers were calculated between the R^{min} value used in the RMC simulations and R^{max}, which was determined by examining the crystal structures, the pair-correlation functions, and the expected geometry of the tellurite polyhedra (Table 2). Table 5 lists only the coordination numbers involving Te and O because the M−O values were constrained during model construction and the M−M correlations were obtained only indirectly, and only in the case of sodium.[16]

The Te−O coordination number represents the most commonly measured feature of tellurite glasses, because it reveals the most information about the structure of the tellurite network. One surprising result is that for the Li and Na tellurite glasses the Te−O coordination number did not decrease significantly as modifier was added, but instead was nearly constant. This constancy indicates that the distribution of three and four coordinate tellurite units is relatively constant, contrary to the accepted view that the glasses change from primarily four-coordinate tellurite tbp's to three-coordinate tp's as modifier is added. This behavior will be examined in greater detail when we discuss the distribution of Q_m^n species in the glasses. Only the potassium glasses appear to follow the generally accepted breakdown of four coordinate species to three coordinate species.

4.3. Tellurite Polyhedra from RMC Models. Defining precisely the structures present in tellurite crystals and glasses is difficult in some cases because of the dispersion in Te−O bond lengths due to charge compensation and weak bonding interactions. Using the ionic radii[30] of Te and O leads to a Te−O bond length of 1.95 Å, whereas using the covalent radii[31] results in a Te−O bond length of 2.09 Å. Te−O interactions between 2.5 and 2.9 Å are often described in terms of secondary or weak bonding. It has been previously established[22,32,33] in this research group, based on the crystal structures described above, that Te−O bond distances between 1.8 and 2.36 Å are bonding in nature and secondary or weak bonding Te−O interactions occur between 2.36 and 2.5 Å. The precise definition of what is considered a bond is necessary in order to use the RMC algorithm to model the glasses, and to analyze the resulting models.

TABLE 6: Distribution of Q_m^n Species in Alkali Tellurite Glasses $(M_2O)_x(TeO_2)_{1-x}$[a]

composition	Q_4^4	Q_4^3	Q_3^2	Q_3^1	Q_3^0	Q_{other}
$(Li_2O)_{0.15}(TeO_2)_{0.85}$	27.3	25.3	30.1	8.6	1.6	7.2
$(Li_2O)_{0.20}(TeO_2)_{0.80}$	18.0	25.7	31.5	15.8	2.9	6.1
$(Li_2O)_{0.25}(TeO_2)_{0.75}$	17.7	29.6	25.5	19.1	3.2	4.9
$(Na_2O)_{0.12}(TeO_2)_{0.88}$	35.2	28.5	25.7	4.8	0.6	5.2
$(Na_2O)_{0.15}(TeO_2)_{0.85}$	26.3	30.2	30.0	8.3	0.8	4.5
$(Na_2O)_{0.20}(TeO_2)_{0.80}$	25.8	31.4	21.9	13.5	3.7	3.9
$(Na_2O)_{0.25}(TeO_2)_{0.75}$	21.6	35.0	21.3	16.4	4.5	1.1
$(Na_2O)_{0.28}(TeO_2)_{0.72}$	23.8	39.9	13.2	15.7	6.1	1.3
$(K_2O)_{0.10}(TeO_2)_{0.90}$	22.9	23.5	33.1	9.9	1.6	9.1
$(K_2O)_{0.20}(TeO_2)_{0.80}$	11.5	18.1	40.3	21.8	3.2	5.0
$(K_2O)_{0.25}(TeO_2)_{0.75}$	5.4	12.8	35.8	30.8	11.0	4.2

[a] Plots showing the distribution of Q_m^n species are shown in Figure 8.

A major difference between the models presented here and previous models for the alkali tellurite glasses is the use of all five tellurite units shown in Figure 1. In particular, earlier models have most frequently excluded the Q_3^2 polyhedron. This unit is in fact present in all of the alkali tellurite crystal structures at the 20 mol-% modification level.[22] It has been argued[17,18] that this unit should be excluded based on the fact that the theoretically predicted Raman resonances[19] for the Q_3^2 unit, at 775 and 870 cm^{-1}, are absent from the glasses.[13] We found, however, that the Raman spectrum of the most relevant model crystalline material, $Na_2Te_4O_9$, also shows no features at these frequencies.[33] This material includes Q_3^2 units,[22] and its Raman spectrum includes a strong band at 825 cm^{-1}, medium bands at 800 and 750 cm^{-1}, and a weak band at 700 cm^{-1}, as well as numerous lower frequency bands.[33] This lack of agreement with calculation[19] suggests that the theoretical prediction of the Raman spectrum is in error. Finally, we found that explicitly excluding the Q_3^2 unit results in models that do not fit diffraction data for the glasses; all five units are necessary to achieve satisfactory fits.

The distributions of Q_m^n units for the alkali tellurite glasses are presented in Table 6 and shown in Figure 8(a−f). The last column in Table 6 is labeled Q_{other} and represents the tellurite units found in the models that were not included in the list of constraints; these made up typically about 5% of the total. The majority (> 95%) of these species were Q_3^3 units, and they persisted at low levels even after the model χ^2 reached a steady value, independent of the starting configuration. In general, such species can be removed "by hand",[34] but that was not done here, because the Q_3^3 units are only one oxygen bond away from the Q_4^3 and Q_3^2 units and could reasonably be counted as either. Examining the distribution of individual Q_m^n species reveals only a few general trends. Initially the Q_4^4 species decrease

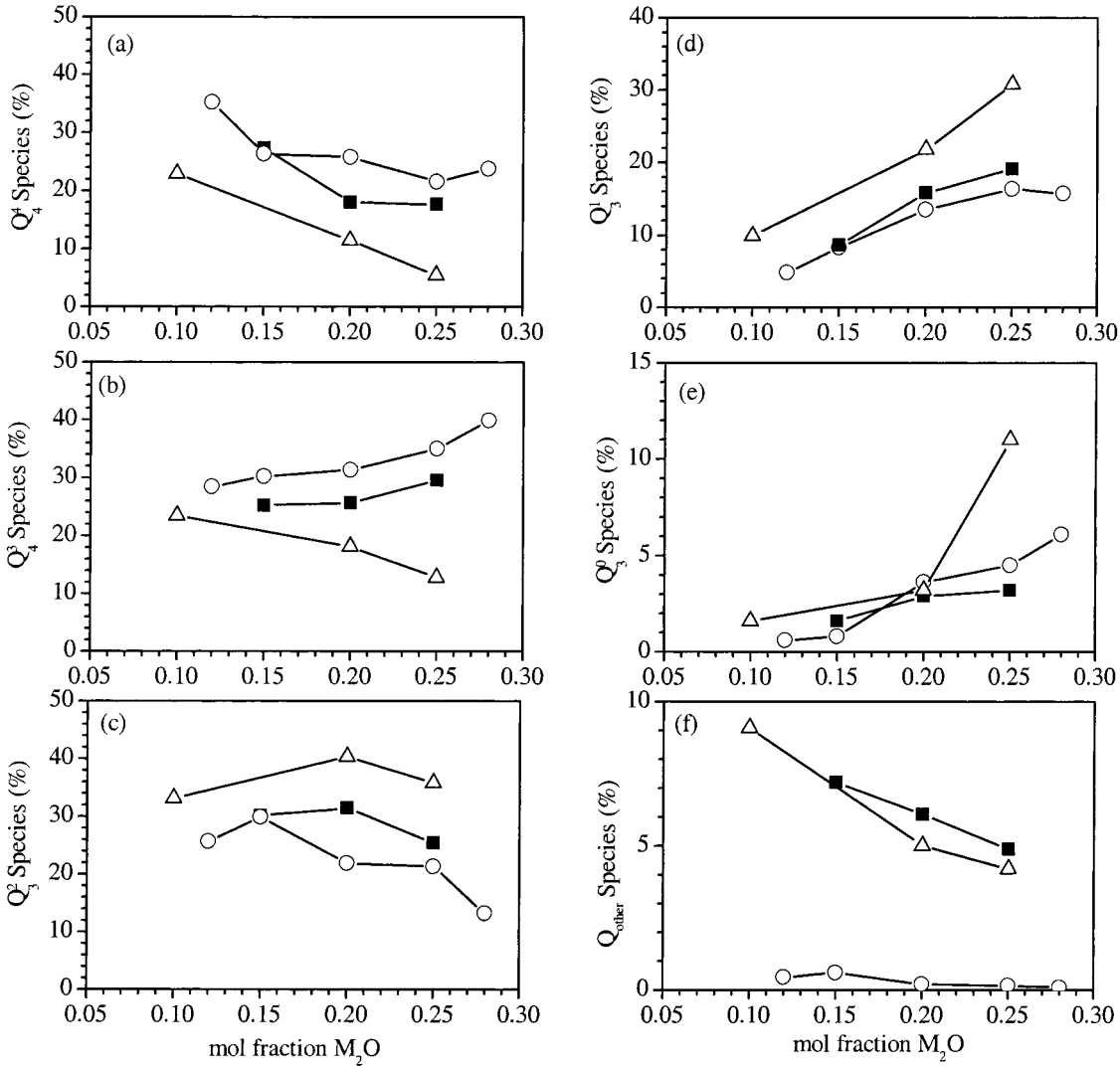

Figure 8. Q_m^n distribution for the alkali tellurite glasses: ■ Li, ○ Na, and △ K.

slightly and then remain level for the Li and Na glasses, while decreasing steadily for the K glasses as the modifier concentration increases. The Q_4^3 species increase for the Li and Na glasses as modifier is added but decrease for the K glasses. The Q_3^2 species increases initially and then decreases for as modifier is added. The Q_3^1 and Q_3^0 species increases steadily as modifier is added for all of the glasses. The trends in the Q_m^n distribution depend on the identity of the cation: Li and Na glasses appearing similar while the K glasses show distinct differences. The causes for these differences will be discussed below.

Overall only the broadest conclusions can be obtained by examining the distribution of individual Q_m^n units. Instead we need to group the Q, units based on two parameters: the Te−O coordination number and the charge balance between the modifier cations and the tellurite network. These parameters are the same two parameters that control the distribution of tellurite species in previous models, but the results are more complex because we have not excluded the Q_3^2 and Q_3^0 species.

Figure 9 shows the distribution of three ($Q_3^2 + Q_3^1 + Q_3^4$) and four ($Q_4^4 + Q_4^3$) coordinate tellurite species. According to earlier models there should be a gradual conversion from four coordinate species to three coordinate species as modifier is added. In fact, the distribution for the Li and Na glasses appears quite flat and actually increases slightly at the highest modifier level. In contrast the K glasses follow the standard paradigm. The principal factor controlling the distribution of thre- and four-coordinate units is the Te−O pair-correlation function and the resulting Te−O coordination number. Thus, the diffraction data does not require a decrease in the Te−O coordination number for the Li and Na glasses as would be expected, but does for the K glasses, and this is reflected in the distribution of Q_m^n units.

The second factor controlling the distribution of Q_m^n species is a charge balance constraint which requires positively charged modifier atoms be balanced by a negative charge on the network. This effect on the Q_m^n distribution is clearly shown in Figure 10a−b where the Q_m^n species are grouped into neutral ($Q_4^4 + Q_3^2$), singly charged ($Q_3^4 + Q_3^1$), and doubly charged (Q_3^0, Figure 8e) species. As expected, the steady decrease of the neutral species is clearly offset by the increase in the singly and doubly charged species.

The resulting individual Q_m^n distributions in tellurite glasses are significantly more complicated than the distribution of Q^n species in typical glass formers such as SiO_2, and P_2O_5. We can now attribute this complexity to two factors. First, both three- and four-coordinate tellurite units are allowed, and second, charge compensation can be achieved with both three- and four-coordinate species. Thus, the distribution of individual tellurite species is harder to predict than the distribution of the tellurite

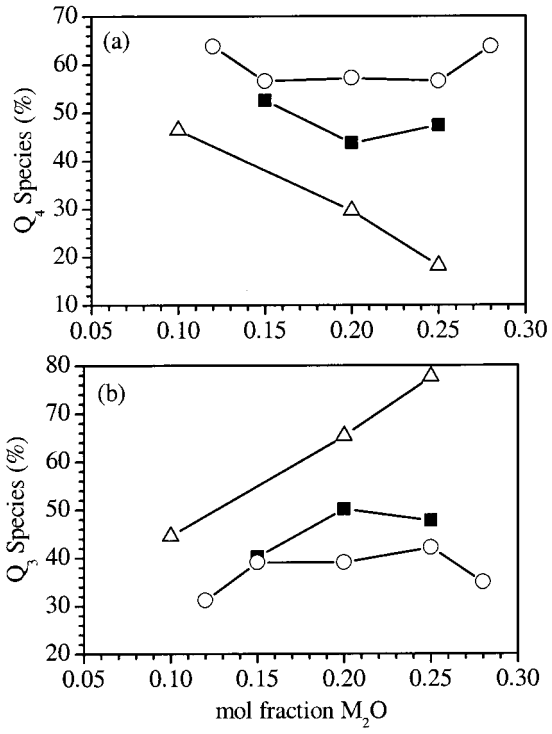

Figure 9. (a) Distribution of four-coordinate (Q_4^4) and (b) three-coordinate ($Q_3^{0,1,2}$) tellurite units in alkali tellurite glasses: ■ Li, ○ Na, and △ K.

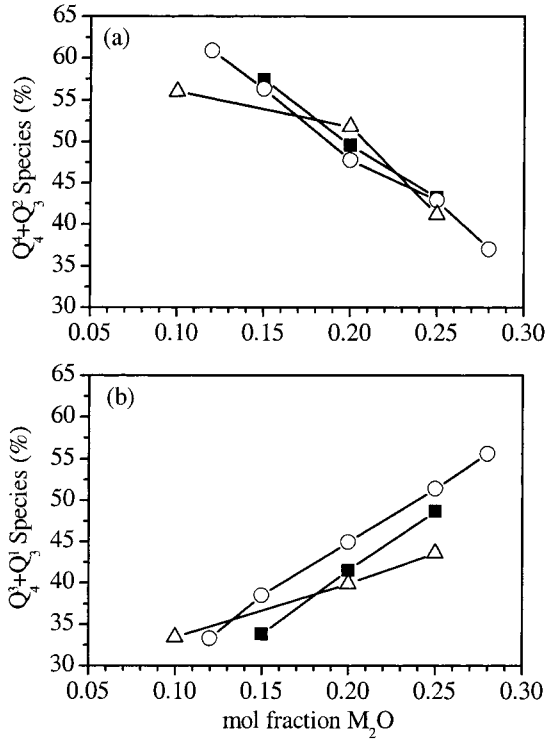

Figure 10. The distribution of Q_m^n species in the alkali tellurite glasses (■ Li, ○ Na, and △ K) grouped by the charge on the tellurite unit. (a) Neutral species ($Q_4^4 + Q_3^2$). (b) Singly charged species ($Q_4^3 + Q_3^1$). For the double charged species (Q_3^0) see Figure 8e.

species grouped by coordination number and charge. The trends in individual Q_m^n species discussed above as a function of modifier content and concentration can now be explained. For the Q_3^4 species in the Li and Na glasses the Te−O coordination number remains relatively constant, thus the Q_4^3 and Q_3^1 species are equally favored, while in the K glasses the Te−O coordination number decreases steadily resulting in Q_3^1 species being favored over Q_4^3 species. The Te−O coordination number is also the reason the Q_4^4 species in the Li and Na glasses do not have to decrease as modifier is added, whereas in the K glasses a decrease is required. The cause of the fluctuations in the Q_3^2 units is more difficult to understand, but is likely due to the interaction between the Te−O coordination number and the charge distribution. In any event, it is clear that K acts more like a traditional modifier than does Na or Li. Since K has the lower field strength, it seems more likely that this difference is due to its larger size. This conjecture is reasonable in light of the relatively small difference in electron density around bridging and nonbridging oxygen in tellurites, as opposed to silicates; in other words, in tellurites all oxygen, bridging or not, are similar and thus direct ionic interactions should be less dominant. Moreover, O−Na and O−Li interaction distances are fairly similar to those of Te−O bonds (about 2.0−2.4 Å in each case), whereas K−O distances are typically 2.7 Å. Hence, K may disrupt the network more strongly just due to size mismatch than do Na and Li, despite its weaker field strength.

4.4. Polyhedral Complexity. The Q_m^n distributions illustrated in Figure 8 do not provide by themselves a simple answer to why the modified glasses become so resistant to devitrification. What is needed is a function that characterizes the distribution more broadly, without bias toward one type of unit or another. We suggest that the key feature governing the resistance to devitrification as a function of composition is the difference between the crystal and glass polyhedral distributions, and in particular the complexity of the distribution of units rather than the presence or absence of certain species. To characterize the distributions we propose use of the following function:

$$\sigma = -\sum [Q_m^n] \ln [Q_m^n] \tag{1}$$

where $[Q_m^n]$ is the fraction of species Q_m^n, and the sum is over all species in the glass. We choose this function because it attains its maximum for an even distribution of unit types, and its minimum if the distribution is dominated by any one type, regardless of which. It thus measures the complexity of the distribution of polyhedra in an unbiased way. It obviously resembles an entropy, but we use it here simply as a way of distinguishing distributions of Q_m^n species that are largely uniform from distributions that are concentrated in one or two types, and to compare these distributions with those in crystals of similar composition.

It is of interest to compare the values of σ derived from the models to those obtained from the crystal structures and to the maximum range of σ. The minimum value of σ, namely 0, is obtained when only one Q_m^n species is present, for example in TeO_2 (Q_4^4 only) and M_2TeO_3 (Q_4^4only). Note also that the Q_m^n distributions satisfy two constraints, due to the sample composition. First, each Q species indicates a single tellurium atom, so

$$\sum [Q_m^n] = 1 \tag{2}$$

Second, the different Q species contain different numbers of oxygen atoms, which must be in the correct ratio to the tellurium at a given modifier content x. This restriction leads to

$$2[Q_4^4] + \frac{5}{2}[Q_4^3] + 2[Q_3^2] + \frac{5}{2}[Q_3^1] + 3[Q_3^0] = \frac{2-x}{1-x} \tag{3}$$

The function $\sigma(x)$ can be maximized subject to these two constraints to describe the maximum diversity of polyhedral

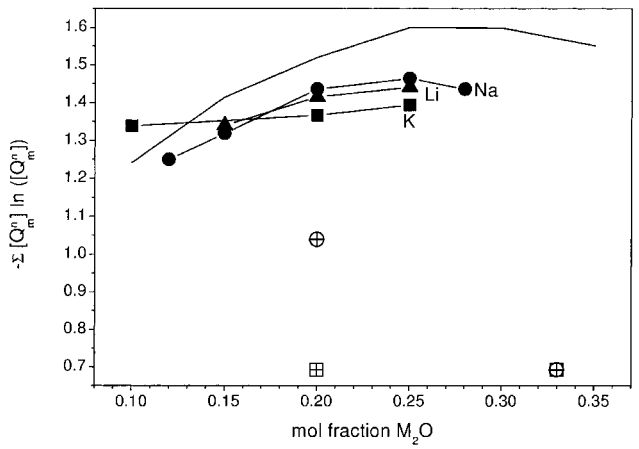

Figure 11. Polyhedral complexity function $\sigma = -\Sigma[Q]\ln[Q]$, as a function of modifier content, for the different glasses. ▲, Li; ●, Na; ■, K. The solid line at top is the maximum σ can take at each composition, given the constraints of total tellurite and oxygen content. σ's for the overlapping crystal compositions are included as well: ⊕, sodium tellurites; ⊞, potassium tellurites.

types at each composition. [Because of the constancy of the oxidation states in this system, eq 3 turns out be equivalent to constraining the charge on the tellurite species to balance the modifier ion content, so this additional constraint adds no new information.]

Figure 11 shows graphs of σ as a function of composition for the different glasses, along with its maximum value based on the constraints of eqs 2 and 3, and the values of σ for crystals in this composition range. This figure shows that the distributions of Q species in the glasses become most uniform at roughly 25 mol-% modifier, and that this behavior is more pronounced, albeit modestly, for the sodium tellurites. The plot also shows that the distribution of polyhedra is in all cases much more complex than that found in crystals of similar composition. Thus, devitrification of these glasses requires significantly greater rearrangements than simple repacking or even redistribution of bridging and nonbridging oxygen at constant coordination number; formation of the crystal from the glass requires significant chemical transformation of Q species, involving changing coordination numbers and bonding types.

5. Conclusions

While this work agrees in some broad features with previous studies of tellurite glass structure, we draw two significantly different conclusions. First, the previously overlooked $O_{2/2}TeO$ unit (Q_3^2 in our nomenclature) is a very significant part of the glass structure. It is found in all alkali tellurite crystals in this composition range, and we find that the diffraction data on the glasses cannot be fit without it. Second, we suggest that the stability of these glasses with respect to devitrification can be explained based on the broad distribution of polyhedra found in the glasses relative to crystals at or near the same compositions. The significance of this distribution is that extensive chemical transformations, not just repackings, are necessary to form the crystals from the glasses upon heating. The large barriers to these processes plus the slow kinetics below T_g effectively prevent these transformations and hence stabilize the glasses.

Acknowledgment. We gratefully acknowledge assistance at IPNS of David Price, Ken Volin, Yaspal Badyal, and Jackie Johnson, and at the APS, of Dean Haeffner and Sarvjit Shastri. This work was supported by the NSF under grant DMR-9508625 and DMR-9870246; work at the APS was supported by the U.S. Department of Energy, BES-Materials Sciences, under contract No. W-31-109-ENG-38.

References and Notes

(1) Varshneya, A. K. *Fundamentals of Inorganic Glasses;* Academic Press: San Diego, 1994.
(2) Heo, J.; Lam, D.; Sigel, Jr., G. H.; Mendoza, E. A.; Hensley, D. A. *J. Am. Ceram. Soc.* **1992**, *75*, 277−281.
(3) El-Mallawany, R. *J. Appl. Phys.* **1992**, *72*, 1774−1777.
(4) Shioya, K.; Komatsu, T.; Kim, H.-G.; Sato, R.; Matusita, K. *J. Non-Cryst. Solids* **1995**, *189*, 16−24.
(5) Dimitriev, Y.; Dimitrov, V.; Arnaudov, M. *J. Mater. Sci.* **1983**, *18*, 1353−1358.
(6) Neov, S.; Kozhukharov, V.; Trapalis, C.; Chieux, P. *Phys. Chem. Glasses* **1995**, *36*, 89−94.
(7) Suzuki, K. *J. Non-Cryst. Solids* **1987**, *95*−*96*, 15−30.
(8) Ueno, M.; Suzuki, K. *Kakuriken Kenkyu Hokoku (Tohoku University)* **1983**, *16*, 49−54.
(9) Neov, S.; Kozhukharov, V.; Gerasimova, I.; Krezhov, K.; Sidzhimov, B. *J. Phys. C* **1979**, *12*, 2475.
(10) Brady, G. W. *J. Chem. Phys.* **1957**, *27*, 300−303.
(11) Nishida, T.; Saruwatari, S.; Takashima, Y. *Bull. Chem. Soc. Jpn.* **1988**, *61*, 1, 4093−4097.
(12) Sekiya, T.; Mochida, N.; Ohtsuka, A.; Tonokawa, M. *J. Non-Cryst. Solids* **1992**, *144*, 128−144.
(13) Tatsumisago, M.; Minami, T.; Kowada, Y.; Adachi, H. *Phys. Chem. Glasses* **1994**, *35*, 89.
(14) Himei, Y.; Osaka, A.; Nanba, T.; Miura, Y. *J. Non-Cryst. Solids* **1994**, *177*, 164−169.
(15) Tagg, S. L.; Youngman, R. E.; Zwanziger, J. W. *J. Phys. Chem.* **1995**, *99*, 9, 5111−5116.
(16) Zwanziger, J. W.; McLaughlin, J. C.; Tagg, S. L. *Phys. Rev. B* **1997**, *56*, 5243−5249.
(17) Sakida, S.; Hayakawa, S.; Yoko, T. *J. Non-Cryst. Solids* **1999**, *243*, 1−12.
(18) Sakida, S.; Hayakawa, S.; Yoko, T. *J. Non-Cryst. Solids* **1999**, *243*, 13−25.
(19) Uchino, T.; Yoko, T. *J. Non-Cryst. Solids* **1996**, *204*, 243−252.
(20) Suehara, S.; Hishita, S.; Inoue, S.; Nukui, A. *Phys. Rev. B* **1998**, *58*, 14124−14126.
(21) Suehara, S.; Yamamoto, K.; Hishita, S.; Aizawa, T.; Inoue, S.; Nukui, A. *Phys. Rev. B* **1998**, *51*, 14919−14922.
(22) Becker, C. R.; Tagg, S. L.; Huffman, J. C.; Zwanziger, J. W. *Inorg. Chem.* **1997**, *36*, 5559−5564.
(23) Koller, H.; Engelhardt, G.; Kentgens, A. P. M.; Sauer, J. *J. Phys. Chem.* **1994**, *98*, 1544−1551.
(24) McLaughlin, J. C.; Zwanziger, J. W. *J. Mol. Graph. Model.* **1999**, *17*, 275−284.
(25) Ellison, A. J. G.; Crawford, R. K.; Montague, D. G.; Volin, K. J.; Price, D. L. *J. Neutron Res.* **1993**, *1*, 61−70.
(26) Williams, A. *X-ray Diffraction Studies of Metallic Glasses*, Thesis, California Institute of Technology, 1980.
(27) McGreevy, R. L.; Pusztai, L. *Mol. Simul.* **1988**, *1*, 359−367.
(28) McGreevy, R. L.; Howe, M. A. *Annu. Rev. Mater. Sci.* **1992**, *22*, 217.
(29) McGreevy, R. L. *Nucl. Instr. Methods Phys. Res. A* **1995**, *354*, 1−16.
(30) Shannon, R. D. *Acta Crystallogr.* **1976**, *A32*, 751.
(31) Miessler, G. L.; Tarr, D. A. *Inorganic Chemistry;* Prentice Hall: New Jersey, 1991.
(32) Tagg, S. L.; Huffman, J. C.; Zwanziger, J. W. *Chem. Mater.* **1994**, 6, 1884−1889.
(33) Tagg, S. L. *Studies of Tellurite Glasses by NMR, Raman Spectroscopy, and Neutron Diffraction*, Thesis, Indiana University, 1997.
(34) Wicks, J. D. *Studies of Disordered Materials*, Thesis, Oxford University, 1993.
(35) Mochida, N.; Takahashi, K.; Nakata, K.; Shibusawa, S. *Yogyo-Kyokai-Shi* **1978**, *86*, 316−326.
(36) Vogel, W. *Glass Chemistry*, 2nd ed.; Springer-Verlag: Berlin, 1994.
(37) Cachau-Herreillat, D.; Norbert, A.; Maurin, M.; Philippot, E. *J. Solid-State Chem.* **1981**, *37*, 352.
(38) Norbert, A.; Cachau-Herreillat, D.; Moret, J. *C. R. Acad. Sci. Paris Ser. C* **1976**, *282*, 511.
(39) Folger, F. *Z. Anorg. Allg. Chem.* **1975**, *411*, 103−110.
(40) Tagg, S. L.; Huffman, J. C.; Zwanziger, J. W. *Acta Chem. Scand.* **1997**, *51*, 118.
(41) Masse, R.; Guitel, J. C.; Tordjman, I. *Mater. Res. Bull.* **1980**, *15*, 431−436.
(42) Anderson, L.; Langer, V.; Strömberg, A.; Strömberg, D. *Acta Crystallogr.* **1989**, *B45*, 344−348.
(43) Loopstra, B. O.; Goubitz, K. *Acta Crystallogr.* **1986**, *C42*, 520−523.